Novel Tracer Method To Measure Isotopic Labeled Gas-Phase Nitrous Acid (HO 15 NO) in Biogeochemical Studies

ARTICLE *in* ENVIRONMENTAL SCIENCE AND TECHNOLOGY · JUNE 2014

Impact Factor: 5.33 · DOI: 10.1021/es501353x · Source: PubMed

9 AUTHORS, INCLUDING:

Dianming Wu
Max Planck Institute for Chemistry
10 PUBLICATIONS **68** CITATIONS
SEE PROFILE

Junfang Cui
Chinese Academy of Sciences
9 PUBLICATIONS **49** CITATIONS
SEE PROFILE

Chunsheng Hu
Institute of Genetics and Developmental Bio…
74 PUBLICATIONS **726** CITATIONS
SEE PROFILE

Environmental Science & Technology

Article

pubs.acs.org/est

Novel Tracer Method To Measure Isotopic Labeled Gas-Phase Nitrous Acid ($HO^{15}NO$) in Biogeochemical Studies

Dianming Wu,[*,†,‡,▲] Christopher J. Kampf,[*,§] Ulrich Pöschl,[§] Robert Oswald,[†,△] Junfang Cui,[∥,⊥] Michael Ermel,[†,△] Chunsheng Hu,[‡] Ivonne Trebs,[†,#] and Matthias Sörgel[†]

[†]Biogeochemistry Department, Max Plank Institute for Chemistry, P.O. Box 3060, 55020 Mainz, Germany

[‡]Key Laboratory of Agricultural Water Research, Center for Agricultural Resources Research, Institute of Genetic and Developmental Biology, The Chinese Academy of Sciences, 050021 Shijiazhuang, Hebei, China

[§]Multiphase Chemistry Department, Max Plank Institute for Chemistry, P.O. Box 3060, 55020 Mainz, Germany

[∥]UCD School of Biosystems Engineering, University College Dublin, Belfield, Dublin 4, Ireland

[⊥]Institute of Mountain Hazards and Environment, The Chinese Academy of Sciences, 610041 Chengdu, Sichuan, China

[▲]University of the Chinese Academy of Sciences, 100049 Beijing, China

[△]Institute for Inorganic and Analytical Chemistry, Johannes Gutenberg University Mainz, 55128 Mainz, Germany

Supporting Information

ABSTRACT: Gaseous nitrous acid (HONO), the protonated form of nitrite, contributes up to ~60% to the primary formation of hydroxyl radical (OH), which is a key oxidant in the degradation of most air pollutants. Field measurements and modeling studies indicate a large unknown source of HONO during daytime. Here, we developed a new tracer method based on gas-phase stripping-derivatization coupled to liquid chromatography−mass spectrometry (LC-MS) to measure the ^{15}N relative exceedance, $\psi(^{15}N)$, of HONO in the gas-phase. Gaseous HONO is quantitatively collected and transferred to an azo dye, purified by solid phase extraction (SPE), and analyzed using high performance liquid chromatography coupled to mass spectrometry (HPLC-MS). In the optimal working range of $\psi(^{15}N) = 0.2-0.5$, the relative standard deviation of $\psi(^{15}N)$ is <4%. The optimum pH and solvents for extraction by SPE and potential interferences are discussed. The method was applied to measure $HO^{15}NO$ emissions from soil in a dynamic chamber with and without spiking ^{15}N labeled urea. The identification of $HO^{15}NO$ from soil with ^{15}N urea addition confirmed biogenic emissions of HONO from soil. The method enables a new approach of studying the formation pathways of HONO and its role for atmospheric chemistry (e.g., ozone formation) and environmental tracer studies on the formation and conversion of gaseous HONO or aqueous NO_2^- as part of the biogeochemical nitrogen cycle, e.g., in the investigation of fertilization effects on soil HONO emissions and microbiological conversion of NO_2^- in the hydrosphere.

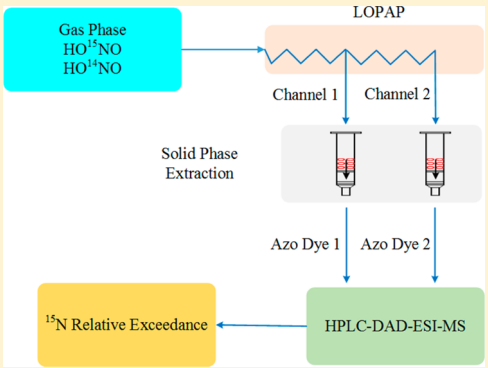

INTRODUCTION

In the lower atmosphere, nitrous acid (HONO) contributes up to ~60% to the primary formation of hydroxyl radical (OH), which is a key oxidant in the degradation of most air pollutants.[1−3] Upon reaction with tobacco smoke, HONO can also form carcinogens and is thus linked to health risks of indoor air pollution.[4]

During daytime, HONO undergoes rapid photolysis, and most field measurement and modeling studies indicate a large unknown source of HONO.[5−9] This unknown source has been tentatively attributed to photosensitized reduction of nitrogen dioxide on humic acid,[10] nitric acid photolysis on surfaces,[11] photolytically enhanced nitrogen dioxide (NO_2) conversion on the ground,[6] anion catalyzed NO_2 conversion,[12] or the photolysis of ortho-nitrophenols.[13] Another potential explanation is the release of HONO from biogenic soil nitrite.[14,15] Large quantities of HONO may be released from a chemical equilibrium of acid−base reaction and gas−liquid partitioning controlled by the temperature, water content, nitrite concentration, and pH of soil,[14] and soil ammonia-oxidizing bacteria (AOB) may release even more HONO than the chemical equilibrium.[16] Soil samples from arid and arable areas as well as peatlands were found to emit HONO in quantities comparable to the emissions of nitric oxide (NO).[16,17]

Several instruments based on spectroscopic methods, (e.g., refs 18−21) and wet chemistry methods have been developed to determine HONO mixing ratios in the atmosphere (e.g., refs

Received: March 19, 2014
Revised: June 16, 2014
Accepted: June 22, 2014

   dx.doi.org/10.1021/es501353x | Environ. Sci. Technol. XXXX, XXX, XXX−XXX

22−25). A very sensitive and reliable technique is the so-called Long Path Absorption Photometer (LOPAP).[26,27] HONO is sampled quantitatively by two stripping coils in series with an efficiency of about 98% in the first coil due to a fast reaction forming the diazonium ion which is the precursor of the azo dye. Hence, potential interferences by species that are not quantitatively removed in the first coil can be detected by the signal from the second coil, and measured values are subsequently corrected for. The instrument measures the light absorption by the azo dye which is formed through the derivatization of HONO by sulfanilamide (SA) and N-(1-naphthyl)-ethylenediamine dihydrochloride (NED), which are Griess type reagents previously used in the analysis of nitrogen dioxide.[28] A similar technique of coil sampling is used to detect the derivated HONO by high performance liquid chromatography (HPLC).[25,29]

The stable nitrogen isotope ^{15}N has been widely used to study biogeochemical N transformation processes in ecosystems.[30−32] ^{15}N labeled nitrite and nitrate were measured by different methods and instruments, e.g., in biological fluids by gas chromatography−mass spectrometry (GC-MS),[33] in seawater by continuous flow isotope ratio mass spectrometry (CF-IRMS),[34] and in various aqueous samples by the sample preparation unit for inorganic nitrogen and mass spectrometer (SPINMAS) technique.[35] The ^{15}N in nitrogen gases, like NO, NO_2, nitrous oxide (N_2O), and nitrogen (N_2), were also determined in a number of studies (e.g., refs 36−39).

However, due to the reactivity, solubility, and low mixing ratios of HONO in the atmosphere, up to now a method to measure the ^{15}N isotope ratio of HONO ($[HO^{15}NO]/[HO^{14}NO]$) is lacking. In this work, we present a new method (gas-phase stripping-derivatization coupled to liquid chromatography−mass spectrometry (LC-MS), LOPAP-HPLC-MS) to determine the ^{15}N relative exceedance ($\psi(^{15}N)$, see ref 40) of the HONO in the gas-phase. The principle of this method is to convert $HO^{15}NO$ to the corresponding ^{15}N azo dye through a Griess reaction during LOPAP analysis and subsequent isotope ratio measurement by HPLC-MS.

EXPERIMENTAL SECTION

Gas Sampling. Gaseous HONO was sampled and analyzed using a commercial LOPAP instrument (LOPAP-03, QUMA Elektronik & Analytik, Germany), which was described in detail previously (see ref 23). Briefly, the HONO from the sample gas flow was quantitatively and continuously sampled into the acidic SA solution and immediately converted to a diazonium ion inside a two channel stripping coil (channel 1: HONO absorption channel; and channel 2: reference channel). The SA solution (58 mM SA in 1 M hydrochloric acid) was pumped continuously to the stripping coil and, after stripping HONO, flushed back to the instrument where it was mixed with 0.39 mM NED to form the azo dye (see the following reaction of the $HO^{15}NO$ derivatization):

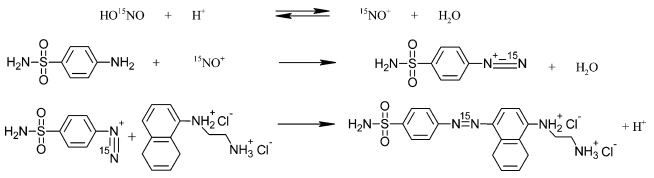

To determine the HONO gas-phase concentrations the dye solutions are passed through a 2−3 m long Teflon AF tubing, a so-called liquid core waveguide, which acts as an absorption cell. The solutions from channels 1 and 2 were collected separately in 5 mL volumetric flasks after the photometric measurement and used for the subsequent analysis of the $\psi(^{15}N)$ of the HONO produced by the experiments.

Sample Purification. The azo dye solution, which was collected from the LOPAP instrument, was purified by reversed-phase solid phase extraction (SPE, DSC-18, Sigma-Aldrich, USA). The following procedure was applied: 1) the pH of the azo dye solution was adjusted to ∼5.5 (the color of the solution changed from red to pink) using 1 M NaOH (VWR International, Germany); 2) the solution was diluted to 20 mL using ultrapure water (18.2 MΩ·cm water, PURELAB Option-Q, ELGA LabWater, UK); 3) preconditioning of the SPE column with 2 mL of acetonitrile (HPLC gradient grade, Carl Roth, Germany) and 2 mL of ultrapure water; 4) extraction of the sample solution (one drop per 2 to 3 s); 5) washing of the extracted sample material using 2 mL of ultrapure water (removal of inorganic ions); and 6) elution of the azo dye from the SPE column using 35/65 (v/v) of acetonitrile (ACN)/0.1% (v/v) trifluoroacetic acid in water (TFA, for liquid chromatography, Merck, Germany) into a 2 mL volumetric flask.

HPLC-MS Analysis. The extracted azo dye samples were analyzed by HPLC-DAD-ESI-MS (Agilent Technologies 1200 series, Agilent technologies, USA). The system consisted of a binary pump (G1379B), autosampler with thermostat (G1330B), column thermostat (G1316B), photodiode array detector (DAD; G1315C), and electrospray ionization quadrupole mass spectrometer (ESI-MS, G6130B). Chemstation software (Rev. B.03.02, Agilent technologies, USA) was used for system control and data analysis. A reversed-phase analytical column (Agilent XDB-C18, 50 mm × 4.6 mm inner diameter, 1.8 μm particle size, Agilent Technologies, USA) was used for chromatographic separation. Eluents were 0.1% TFA in water (Eluent A) and ACN (Eluent B). Gradient elution was applied at a flow rate of 500 $\mu L\ min^{-1}$. For each chromatographic run, the solvent gradient started with 25% B for 1 min followed by a linear gradient to 90% B within 3.5 min, holding this composition for another 3.5 min, flushing back to 3% B within 1 min, and column re-equilibration for 6 min before the next run. The injection volume was 20−80 μL during the method development, and 80 μL was used for soil experiment sample analysis. Each chromatographic run was repeated three times. The acquired wavelength range was 200−800 nm for DAD detection. Detection and reference wavelengths for azo dye analysis were 540 and 700 nm with bandwidths of 10 and 60 nm, respectively. The ESI-MS instrument was operated in the positive ionization mode (ESI+) with an ionization voltage of 1750 V and a fragmentor voltage of 175 V at a dry gas temperature of 300 °C. MS spectra were recorded in scan mode (m/z 50−500) and single ion monitoring mode (m/z 370.1, 371.1, 372.1, and 373.1).

Calibration. The azo dye concentration and the $\psi(^{15}N)$ in the azo dye samples were calibrated using the DAD and MS detectors, respectively. Aqueous sodium nitrite standard solution (Carl Roth, Germany) was used to prepare the azo dye concentration calibration curve. A series of nitrite working standard solutions containing 0 to 18.1 μM sodium nitrite were prepared before use from a 14.5 mM sodium nitrite standard, which was stored at 4 °C. Five mL of the working solutions were mixed with equal amounts of 58 mM SA in 1 M hydrochloric acid and additional 5 mL of 0.39 mM NED to form the azo dye calibration solutions. Unlabeled and ^{15}N labeled sodium nitrite (98%+, Cambridge Isotope Laboratories,

dx.doi.org/10.1021/es501353x | Environ. Sci. Technol. XXXX, XXX, XXX−XXX

USA) solutions of the same concentration were mixed together in varying ratios and processed as mentioned before to obtain the $\psi(^{15}N)$ calibration standards. The sample purification and analysis were carried out as described above.

^{15}N Relative Exceedance Calculation. The $\psi(^{15}N)$ of the azo dye was calculated according to refs 33 and 41. Due to the natural isotope distribution of the unlabeled azo dye (M ($C_{18}H_{19}O_2N_5S$) = 369.1 g mol^{-1}), the ESI+ mass spectra include the protonated molecular ions ($[M + H]^+$, *M*) *M + 0*, *M + 1*, *M + 2*, and *M + 3*. Unlabeled azo dye working standards were used to analyze the isotope distributions at different azo dye concentrations. The ratio of the *M + 1*, *M + 2*, and *M + 3* ions for a given azo dye concentration was found to show slight daily variations, likely due to small fluctuations of the conditions in the ion source. Peak areas (mAU) of the extracted ion chromatograms (EIC) for *m/z* 370, *m/z* 371, *m/z* 372, and *m/z* 373 were used to calculate the normalized signal ratios of unlabeled azo dye standards shown in Table 1.

Table 1. Normalized Isotope Distribution of the Unlabeled Azo Dye

parameter	value			
ion monitored (*m/z*)	370	371	372	373
mass	*M*	*M + 1*	*M + 2*	*M + 3*
intensity	1.00	0.244[a]	0.072[a]	0.011[a]

[a]Average data obtained from different azo dye concentrations.

Since the liquid-chromatographic separation represents an isotope fractionation process, it is important to take into account the whole peak area of the EICs of interest for the analysis of isotope distributions by HPLC-MS.[42]

Using the values from Table 1, the $\psi(^{15}N)$ is calculated according to Green et al. (1982)[33] as

$$\psi(^{15}N) = \frac{^{371}AD - 0.244\,^{370}AD}{^{370}AD + {}^{371}AD - 0.244\,^{370}AD + 0.072\,^{370}AD + 0.011\,^{370}AD} \quad (1)$$

where ^{370}AD and ^{371}AD are the peak areas of the EICs for *m/z* 370 and *m/z* 371, respectively.

This is simplified to

$$\psi(^{15}N) = \frac{R - 0.244}{R + 0.839} \quad (2)$$

where $R = (^{371}AD)/(^{370}AD)$, and ^{370}AD and ^{371}AD are the peak areas of the EICs for *m/z* 370 and *m/z* 371, respectively.

Soil Experiments. The method was applied for the $\psi(^{15}N)$ analysis of HONO emissions from soil samples spiked with ^{15}N labeled urea ($CO(^{15}NH_2)_2$, 98%+, Cambridge Isotope Laboratories, USA). Soil samples were collected from a long-term tillage field (winter wheat and summer corn rotation) in Lyons Estate (53°18′32.85″N, 60°32′31.62″W), Co. Kildare, Ireland. The soil was a clay loam (sand 30.4%, silt 39.7%, clay 29.9%; bulk density 1.47 g cm^{-3}; total porosity 44.3%; pH (H_2O) 7.2; organic carbon 2.06%; total nitrogen 0.31%; NH_4^+-N 1.4 mg kg^{-1}; NO_2^--N 0.27 mg kg^{-1}; NO_3^--N 6.8 mg kg^{-1}) and was classified as Gray Brown Podzolic soil (Haplic Luvisol soil unit and Luvisol major soil grouping in FAO/UNESCO system, belongs to Alfisol soil order in the USDA system).[43] After being air-dried and passed through a 2 mm sieve, the soil was stored at 4 °C before being used for an experiment. Fifty grams of a homogeneously mixed soil sample were placed in a Petri dish (inner diameter = 88 mm) and wetted with ultrapure water to water holding capacity (WHC, see ref 16). The Petri dish was placed into a dynamic chamber made of Teflon (volume 47 L), which was located in a temperature controlled (25 °C) climate cabinet, and flushed with purified dry air at a flow rate 8 L min^{-1}. Mixing ratios of HONO, NO, NO_2, O_3, CO_2, and H_2O were monitored in the chamber headspace by the LOPAP, a NO_x chemiluminescence analyzer (Model 42i-TL, Thermo Scientific, USA), an Ozone analyzer (Model 49i, Thermo Scientific, USA), and a LI-COR (Model 840A, LI-COR, USA), respectively. This setup was described in detail elsewhere.[16] The limit of detection was ∼5 ppt for HONO, ∼80 ppt for NO, and ∼280 ppt for NO_2, respectively. Fluxes of HONO and NO were calculated based on the following formula (see ref 16)

$$F = \frac{Q}{A} * \frac{1}{V_m} * (\chi_{out} - \chi_{in}) \quad (3)$$

where *F* is the flux of HONO and NO (nmol m^{-2} s^{-1}), *Q* is the purging flow rate (m^3 s^{-1}), χ_{out} and χ_{in} are the headspace mixing ratio at outlet and inlet of the chamber (ppb), *A* is the area of soil (m^2), and V_m is the molar volume of air (m^3 mol^{-1}).

The corresponding errors of the fluxes were calculated using Gaussian error propagation.[16] Soil gravimetric water content (SWC) was calculated from the loss of water during the experiment and then normalized to the WHC.[16] For the experiment with ^{15}N labeled urea, 8.62 mL of $CO(^{15}NH_2)_2$ solution with a concentration of 16.4 mM was added to the soil sample before the addition of ultrapure water and continuing the experiment as described above. The addition of urea corresponds to 150 kg ha^{-1} (in terms of N) fertilizer applied in the field. The azo dye solutions from channels 1 and 2 of the LOPAP instrument were collected, and $\psi(^{15}N)$ of the emitted HONO was analyzed according to the presented procedure. The $\psi(^{15}N)$ of HONO caused by fertilizing was calculated using the $\psi(^{15}N)$ of HONO from the fertilized soil experiment and subtracting the values obtained from the unfertilized soil experiment. Before and after the soil measurements, soil nutrient (ammonium, nitrite, and nitrate) contents were analyzed according to the ISO/TS 14256-1 standard procedure.

RESULTS AND DISCUSSION

A detailed characterization of the collection efficiency, potential interferences (NO_2, O_3, PAN, HNO_3, etc.), and instrument parameters of the LOPAP were presented by Kleffmann and co-workers.[23,26,27] Here, we discuss the analytical method development of $\psi(^{15}N)$ determination of HONO by HPLC-MS.

Azo Dye Extraction and Chromatography. Azo dye recovery was found to be affected by solution pH and extraction solvent composition. Too high or too low pH of the sample solution decreased the azo dye recovery, e.g. by protonation, which prevented or strongly reduced azo dye retention on the SPE column. Hence, the pH of the azo dye sample was adjusted to ∼5.5 before SPE extraction, which is the value of the change of color of the azo dye. Results of recovery experiments showed that the best extraction efficiency was obtained using 35/65 (v/v) of ACN/0.1% TFA (Figure S1) as extraction solvent.

Typical chromatograms of the ^{15}N labeled azo dye are shown in Figure S2. The eluent gradient for chromatographic

dx.doi.org/10.1021/es501353x | Environ. Sci. Technol. XXXX, XXX, XXX−XXX

separation was optimized to ensure a chromatographic resolution of the azo dye signal that allows for a reliable use of the automatic integration tool provided in the Chemstation software, while maintaining short overall run times (<20 min). The retention time of the azo dye was 2.8 min.

Method Blanks and Calibration. Method blanks for calibration purposes were obtained by applying the derivatization and SPE procedure as discussed in the Experimental Section without adding sodium nitrite. The method blanks therefore include all relevant factors that could affect the azo dye concentrations, e.g. exposure to ambient air, impurities in water and reagents, SPE column, matrix effects, measurement artifacts, and HPLC-MS background signal. The average (n = 3) concentrations of the method blanks detected during the method development were 0.11 μM (corresponding to ~0.4 ppb HONO in the gas-phase for the experimental setup described above). The detection limit was found to be 0.078 μM (3σ method).

A calibration curve for unlabeled aqueous sodium nitrite solution with concentrations ranging from 0 to 19 μM is shown in Figure 1. The error bars represent the standard deviation of

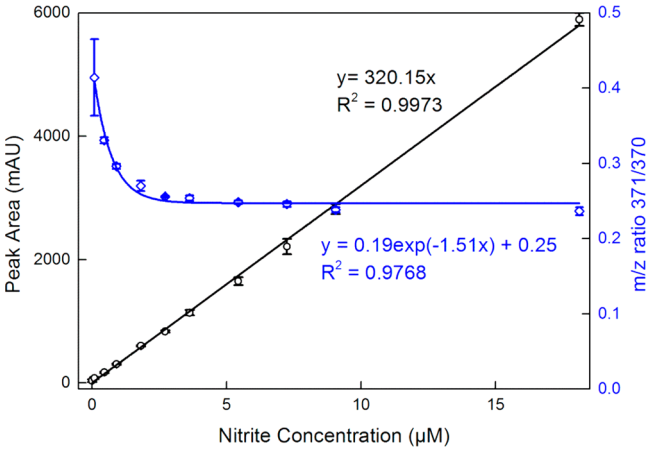

Figure 1. Calibration curve for unlabeled nitrous acid and concentration dependence of m/z ratio 371/370. Open circles (black) represent the 540 nm signal peak area (mAU) of azo dye for different nitrite concentrations. Open diamonds (blue) correspond to the m/z ratio of 371/370. Error bars denote the standard deviation (n = 3).

three calibration curves obtained on a monthly basis. The values agree within 5% of the peak area, thus proving the reproducibility of sample preparation and analysis. The nitrite calibration range corresponds to a HONO gas-phase mixing ratios range of 0–200 ppb measured with the LOPAP.

Despite the good linearity of the concentration calibration, a dependence of the ratio of the signal areas of the EICs of m/z 371 and m/z 370 (termed m/z ratio 371/370 hereafter, which is used to calculate $\psi(^{15}N)$ in eq 2) from the azo dye concentration was observed (Figure 1). The m/z ratio 371/370 decreased from 0.41 to 0.27 with nitrite concentrations increasing from 0.09 μM to 1.81 μM and remained nearly stable at higher concentrations. The lowest observed ratio was 0.23, which is close to the theoretical value of 0.22. A similar behavior was observed for the determination of ^{15}N abundance in ammonium, nitrite, and nitrate by the SPINMAS method, which was attributed to contaminations by atmospheric N_2 for low total N-amounts.[35] In our method, a positive linear relationship (R^2 = 0.97) was found between the m/z ratio 371/370 and the percentage of blank concentration in total nitrite concentration (Figure S3). This suggests that the overestimation of the m/z ratio 371/370 was caused by the method blank at low nitrite concentrations (<1.81 μM). However, as long as the nitrite concentration was above this threshold value, the observed ratio was close to the theoretical value (Figure S3). Hence, the threshold amount of N injected was found to be 2.03 ng (in 80 μL injection volume). This value corresponds to ~5 ppb HONO in the gas-phase measured by the LOPAP.

Figure 2 shows the average $\psi(^{15}N)$ of the calibration curve for four different dye concentrations above the threshold (1.81,

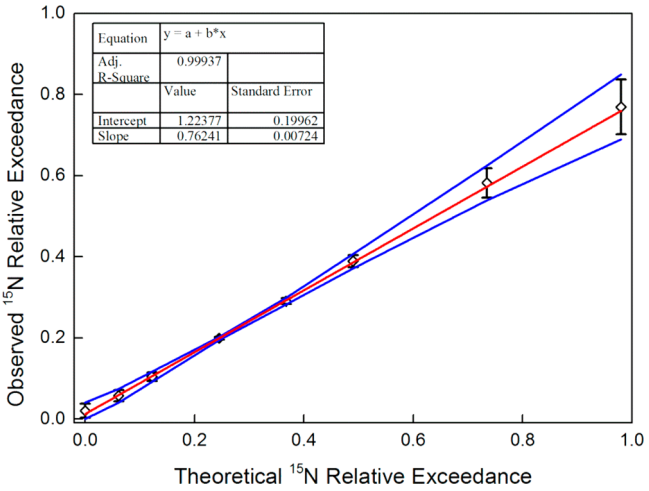

Figure 2. Correlation (y = 0.7624x + 1.2238) between $\psi(^{15}N)$ of calibration standards and measurements by HPLC-MS. Shown are mean values and standard deviations for the analysis of four isotope ratio calibration curves at different dye concentrations (see text). The blue lines show the upper and lower confidence bands (±95%).

4.53, 9.06, and 18.1 μM). The calibration curve of the $\psi(^{15}N)$ is linear (R^2 = 0.9994) but has an optimum range as can be seen from the ±95% confidence bands. The relative standard deviation of the $\psi(^{15}N)$ is <4% between $\psi(^{15}N)$ = 0.2 and 0.5, while it increases to ~10% and ~100% with the $\psi(^{15}N)$ increasing to 0.98 or decreasing to 0, respectively. Therefore, the highest accuracy for deriving the $\psi(^{15}N)$ is obtained within the range of 0.2–0.5.

Notably, the slope of the calibration curve is <1 (0.76). This could be caused by the observed background signal at m/z 370, e.g., in the method blanks. A similar deviation from the 1:1 line was observed in a study of ^{13}C labeled fatty acids analyzed by HPLC-API-MS.[44] To test for the influence of the mass resolution of the instrument on the $\psi(^{15}N)$ analysis, a series of ^{15}N labeled calibration standards ($\psi(^{15}N)$ range from 0–0.49 with a concentration of 0.91 μM) was analyzed using a nano high performance liquid chromatography coupled to quadruple Time-of-Flight mass spectrometry (nanoHPLC-nanoESI-QToF) instrument (mass resolution ~20,000, see the Supporting Information for more details). Using this instrument, the slope of the $\psi(^{15}N)$ calibration curve was found to be 0.8855 (Figure S4). Apparently, less background signal intensity due to higher mass resolution could partly eliminate the cause for the low slope. However, for the proposed application to soil experiments, the results from the low resolution HPLC-MS system were found to be sufficient.

dx.doi.org/10.1021/es501353x | Environ. Sci. Technol. XXXX, XXX, XXX–XXX

Potential Interferences. Due to the concentration dependency of m/z ratio 371/370, factors that might influence nitrite or dye concentration will affect analysis of the $\psi(^{15}N)$. It was reported previously that the absorbance of the azo dye at 540 nm attained its maximum intensity within 2 min.[45,46] We investigated the influence of storage time and temperature on azo dye concentration and its m/z ratio 371/370. The azo dye concentration was found to decrease linearly with time independent of its concentration (Figure S5). Sample storage at 4 °C reduced the concentration decrease over time by a factor ~2 compared to storage at room temperature (RT). For this study, samples were analyzed on the same or the following day of the soil experiments. More importantly, the m/z ratio 371/370 of the dye was found to be unaffected by its decomposition (Figure S5).

Potential interferences from matrix effects were also investigated. The LOPAP reaction solution contains considerably high concentration of SA (58 mM) and NED (0.39 mM). While SA is supposed to be relatively stable, NED is subject to decomposition under irradiated conditions. Hence, samples of 2 mL of 0.39 mM NED solution were exposed to sunlight for 0, 1, 5, 10, 30, and 60 min, respectively, and then analyzed by HPLC-MS with and without addition of 2 mL of 0.91 μM azo dye solution. The results showed that neither the azo dye signal area nor its $\psi(^{15}N)$ was affected by the NED matrix (Table S1).

Application to Soil Experiments. Figure 3 shows calculated HONO and NO fluxes as well as $\psi(^{15}N)$ of HONO emitted during soil measurements conducted with and without fertilizing with ^{15}N labeled urea. The corresponding HONO mixing ratios in the gas-phase were ~7 and ~10 ppb for unfertilized and fertilized soil, respectively, and thus higher than the threshold value of ~5 ppb. The $\psi(^{15}N)$ values in Figure 3 were corrected for the $\psi(^{15}N)$ values of the unfertilized sample. Compared to the unfertilized soil sample, the optimum fluxes of HONO and NO increased from ~15 and ~19 nmol m^{-2} s^{-1} to ~20 and ~24 nmol m^{-2} s^{-1} for the fertilized soil sample, respectively. The hydrolysis of urea to ammonia or ammonium by ammonia-oxidizing bacteria or archaea[47−49] and the subsequent emission of HONO and NO through nitrification[16,50,51] are potentially responsible for the increased fluxes. This finding is supported by measurements of soil nutrients (ammonium, nitrite, and nitrate), which increased by a factor of 12 for ammonium, a factor of 2 for nitrite, while not significantly for nitrate after the soil measurement with the addition of labeled urea (Table S2). This conversion is indicative for microbial processes.[52] The $\psi(^{15}N)$ of HONO caused by fertilizing was in the range of 0.41−0.5 during the soil measurements. Statistical analysis showed that the $\psi(^{15}N)$ values of the emitted HONO, that were measured at SWC below the optimum emission (labeled with b), were significantly higher than the $\psi(^{15}N)$ values close to the optimum emission flux (labeled with a). However, from the AVONA t test no significant difference among the $\psi(^{15}N)$ values labeled with b was found. The change of the $\psi(^{15}N)$ of the emitted HONO during the dry-out of the soil samples can be explained by the depletion of natural nutrient pools over time, increasing microbial activity, or by various sources of HONO emission from soils (AOB combined with chemical equilibrium). The $\psi(^{15}N)$ of the optimum HONO flux caused by fertilizing was ~0.42 and, thus, comparable to the increase of the optimum HONO flux from unfertilized to fertilized soil samples (~38%). These results confirm biogenic HONO emissions from soil,[16] which significantly influence the oxidation capacity of the atmosphere.

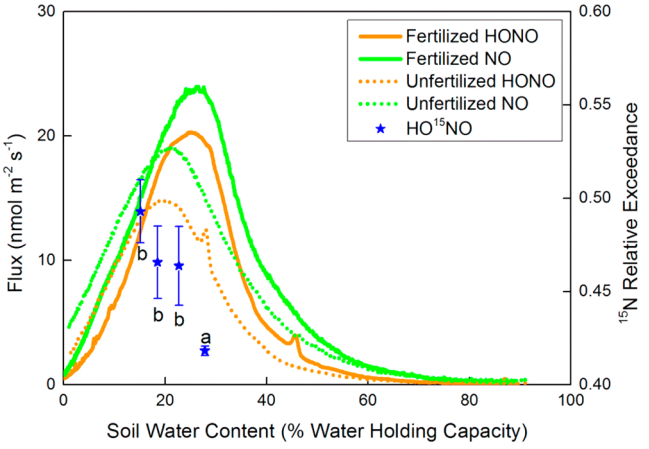

Figure 3. Application of the method to soil measurements. Fluxes of HONO and NO with spiking of ^{15}N labeled urea (solid orange and green line, respectively) and without spiking of ^{15}N labeled urea (dotted orange and green line, respectively). Error bars of HONO and NO fluxes were omitted for clarity, but in general the relative errors determined by error propagation were within 10% of the flux. The $\psi(^{15}N)$ of HONO caused by fertilizing (blue filled stars, difference between the $\psi(^{15}N)$ of fertilized and unfertilized sample) were measured during the dry-out of the soil samples. Error bars are ±95% confidence intervals of the $\psi(^{15}N)$ based on the calibration curve in Figure 3. Means marked by different lowercase letters (a and b, see text) are significantly different from each other at $P < 0.05$ according to the ANOVA t test ($n = 3$).

In conclusion, the presented ^{15}N tracer method provides a new opportunity to study the processes of HONO emission from soils. In the optimal working range of $\psi(^{15}N) = 0.2–0.5$, the relative standard deviation of $\psi(^{15}N)$ is <4%, which is comparable to other ^{15}N tracer studies.[31,53,54] Future investigations should focus on the improvement of the precision of the method, which includes decreasing the injection threshold to detect the $\psi(^{15}N)$ by HPLC-MS. Due to the limitations of our method, the measurement of natural ^{15}N isotope abundances of atmospheric HONO is not possible up to now. Future developments may use nitrogen-free derivatization agents, a high resolution mass spectrometer, or laser techniques to investigate the natural ^{15}N distribution of HONO. The method could potentially be applied for tracer studies in other research fields, such as atmospheric chemistry (e.g., ozone formation from HONO and photolysis of labeled HNO_3), ecohydrology (e.g., refs 55 and 56), and wastewater treatment studies (e.g., potential HONO release during nitrogen and phosphorus removal from ammonium-rich wastewater).

■ ASSOCIATED CONTENT

Supporting Information

Information on the nanoHPLC-nanoESI-QToF setup, typical HPLC-MS chromatograms, the $\psi(^{15}N)$ of calibration curve measured by nanoHPLC-nanoESI-QToF, the effects of solvents, blank concentrations, storage time and temperature, and matrix on the azo dye concentration and its $\psi(^{15}N)$, and the nutrient content before and after measurements; Figures S1−S5 and Tables S1 and S2. This material is available free of charge via the Internet at http://pubs.acs.org.

dx.doi.org/10.1021/es501353x | Environ. Sci. Technol. XXXX, XXX, XXX−XXX

AUTHOR INFORMATION

Corresponding Authors

*Phone: 49 61313056404. Fax: 49 61313056405. E-mail: dianming.wu@mpic.de.

*Phone: 49 61313056206. Fax: 49 61313056405. E-mail: c.kampf@mpic.de.

Present Address

#Centre de Recherche Public - Gabriel Lippmann, Department Environment and Agro-biotechnologies, 41 rue du Brill, L-4422 Belvaux, Luxembourg.

Notes

The authors declare no competing financial interest.

ACKNOWLEDGMENTS

This project was funded by the Max Planck Society and the Max Planck Graduate Center with the Johannes Gutenberg-Universität Mainz (MPGC). We are grateful to Drs. Oliver Spott, Hang Su, and Yafang Cheng for their comments during the method development. We also thank Prof. Dr. Jürgen Kesselmeier, Michael Welling, Nina-Maria Knothe, and Dr. Daniel Plake for supporting our experiments.

REFERENCES

(1) Alicke, B.; Geyer, A.; Hofzumahaus, A.; Holland, F.; Konrad, S.; Pätz, H. W.; Schäfer, J.; Stutz, J.; Volz-Thomas, A.; Platt, U. OH formation by HONO photolysis during the BERLIOZ experiment. *J. Geophys. Res.: Atmos.* **2003**, *108* (D4), 8247.

(2) Volkamer, R.; Sheehy, P.; Molina, L. T.; Molina, M. J. Oxidative capacity of the Mexico City atmosphere – Part 1: A radical source perspective. *Atmos. Chem. Phys.* **2010**, *10* (14), 6969–6991.

(3) Ren, X.; Harder, H.; Martinez, M.; Lesher, R. L.; Oliger, A.; Simpas, J. B.; Brune, W. H.; Schwab, J. J.; Demerjian, K. L.; He, Y.; Zhou, X.; Gao, H. OH and HO_2 Chemistry in the urban atmosphere of New York City. *Atmos. Environ.* **2003**, *37* (26), 3639–3651.

(4) Sleiman, M.; Gundel, L. A.; Pankow, J. F.; Jacob, P.; Singer, B. C.; Destaillats, H. Formation of carcinogens indoors by surface-mediated reactions of nicotine with nitrous acid, leading to potential thirdhand smoke hazards. *Proc. Natl. Acad. Sci. U. S. A.* **2010**, *107* (15), 6576–6581.

(5) Sörgel, M.; Regelin, E.; Bozem, H.; Diesch, J. M.; Drewnick, F.; Fischer, H.; Harder, H.; Held, A.; Hosaynali-Beygi, Z.; Martinez, M.; Zetzsch, C. Quantification of the unknown HONO daytime source and its relation to NO_2. *Atmos. Chem. Phys.* **2011**, *11* (20), 10433–10447.

(6) Wong, K. W.; Tsai, C.; Lefer, B.; Haman, C.; Grossberg, N.; Brune, W. H.; Ren, X.; Luke, W.; Stutz, J. Daytime HONO vertical gradients during SHARP 2009 in Houston, TX. *Atmos. Chem. Phys.* **2012**, *12* (2), 635–652.

(7) Kleffmann, J. Daytime sources of nitrous acid (HONO) in the atmospheric boundary layer. *ChemPhysChem* **2007**, *8* (8), 1137–1144.

(8) Su, H.; Cheng, Y. F.; Shao, M.; Gao, D. F.; Yu, Z. Y.; Zeng, L. M.; Slanina, J.; Zhang, Y. H.; Wiedensohler, A. Nitrous acid (HONO) and its daytime sources at a rural site during the 2004 PRIDE-PRD experiment in China. *J. Geophys. Res.: Atmos.* **2008**, *113* (D14), D14312.

(9) Li, X.; Brauers, T.; Häseler, R.; Bohn, B.; Fuchs, H.; Hofzumahaus, A.; Holland, F.; Lou, S.; Lu, K. D.; Rohrer, F.; Hu, M.; Zeng, L. M.; Zhang, Y. H.; Garland, R. M.; Su, H.; Nowak, A.; Wiedensohler, A.; Takegawa, N.; Shao, M.; Wahner, A. Exploring the atmospheric chemistry of nitrous acid (HONO) at a rural site in Southern China. *Atmos. Chem. Phys.* **2012**, *12* (3), 1497–1513.

(10) Stemmler, K.; Ammann, M.; Donders, C.; Kleffmann, J.; George, C. Photosensitized reduction of nitrogen dioxide on humic acid as a source of nitrous acid. *Nature* **2006**, *440* (7081), 195–198.

(11) Zhou, X.; Zhang, N.; TerAvest, M.; Tang, D.; Hou, J.; Bertman, S.; Alaghmand, M.; Shepson, P. B.; Carroll, M. A.; Griffith, S.; Dusanter, S.; Stevens, P. S. Nitric acid photolysis on forest canopy surface as a source for tropospheric nitrous acid. *Nat. Geosci.* **2011**, *4* (7), 440–443.

(12) Yabushita, A.; Enami, S.; Sakamoto, Y.; Kawasaki, M.; Hoffmann, M. R.; Colussi, A. J. Anion-catalyzed dissolution of NO_2 on aqueous microdroplets. *J. Phys. Chem. C* **2009**, *113* (17), 4844–4848.

(13) Bejan, I.; Abd-el-Aal, Y.; Barnes, I.; Benter, T.; Bohn, B.; Wiesen, P.; Kleffmann, J. The photolysis of ortho-nitrophenols: a new gas phase source of HONO. *Phys. Chem. Chem. Phys.* **2006**, *8* (17), 2028–2035.

(14) Su, H.; Cheng, Y.; Oswald, R.; Behrendt, T.; Trebs, I.; Meixner, F. X.; Andreae, M. O.; Cheng, P.; Zhang, Y.; Pöschl, U. Soil nitrite as a source of atmospheric HONO and OH radicals. *Science* **2011**, *333* (6049), 1616–1618.

(15) Kubota, M.; Asami, T. Source of nitrous acid volatilized from upland soils. *Soil Sci. Plant Nutr.* **1985**, *31* (1), 35–42.

(16) Oswald, R.; Behrendt, T.; Ermel, M.; Wu, D.; Su, H.; Cheng, Y.; Breuninger, C.; Moravek, A.; Mougin, E.; Delon, C.; Loubet, B.; Pommerening-Röser, A.; Sörgel, M.; Pöschl, U.; Hoffmann, T.; Andreae, M. O.; Meixner, F. X.; Trebs, I. HONO emissions from soil bacteria as a major source of atmospheric reactive nitrogen. *Science* **2013**, *341* (6151), 1233–1235.

(17) Maljanen, M.; Yli-Pirilä, P.; Hytönen, J.; Joutsensaari, J.; Martikainen, P. J. Acidic northern soils as sources of atmospheric nitrous acid (HONO). *Soil Biol. Biochem.* **2013**, *67* (0), 94–97.

(18) Perner, D.; Platt, U. Detection of nitrous acid in the atmosphere by differential optical absorption. *Geophys. Res. Lett.* **1979**, *6* (12), 917–920.

(19) Winer, A. M.; Biermann, H. W. Long pathlength differential optical absorption spectroscopy (DOAS) measurements of gaseous HONO, NO_2 and HCNO in the California South Coast Air Basin. *Res. Chem. Intermed.* **1994**, *20* (3–5), 423–445.

(20) Alicke, B.; Platt, U.; Stutz, J. Impact of nitrous acid photolysis on the total hydroxyl radical budget during the Limitation of Oxidant Production/Pianura Padana Produzione di Ozono study in Milan. *J. Geophys. Res.: Atmos.* **2002**, *107* (D22), 8196.

(21) Roberts, J. M.; Veres, P.; Warneke, C.; Neuman, J. A.; Washenfelder, R. A.; Brown, S. S.; Baasandorj, M.; Burkholder, J. B.; Burling, I. R.; Johnson, T. J.; Yokelson, R. J.; de Gouw, J. Measurement of HONO, HNCO, and other inorganic acids by negative-ion proton-transfer chemical-ionization mass spectrometry (NI-PT-CIMS): application to biomass burning emissions. *Atmos. Meas. Tech.* **2010**, *3* (4), 981–990.

(22) Vecera, Z.; Dasgupta, P. K. Measurement of atmospheric nitric and nitrous acids with a wet effluent diffusion denuder and low-pressure ion chromatography-postcolumn reaction detection. *Anal. Chem.* **1991**, *63* (20), 2210–2216.

(23) Heland, J.; Kleffmann, J.; Kurtenbach, R.; Wiesen, P. A new instrument to measure gaseous nitrous acid (HONO) in the atmosphere. *Environ. Sci. Technol.* **2001**, *35* (15), 3207–3212.

(24) Zellweger, C.; Ammann, M.; Hofer, P.; Baltensperger, U. NOy speciation with a combined wet effluent diffusion denuder – aerosol collector coupled to ion chromatography. *Atmos. Environ.* **1999**, *33* (7), 1131–1140.

(25) Zhou, X.; Qiao, H.; Deng, G.; Civerolo, K. A method for the measurement of atmospheric HONO based on DNPH derivatization and HPLC analysis. *Environ. Sci. Technol.* **1999**, *33* (20), 3672–3679.

(26) Kleffmann, J.; Wiesen, P. Technical Note: Quantification of interferences of wet chemical HONO LOPAP measurements under simulated polar conditions. *Atmos. Chem. Phys.* **2008**, *8* (22), 6813–6822.

(27) Kleffmann, J.; Lörzer, J. C.; Wiesen, P.; Kern, C.; Trick, S.; Volkamer, R.; Rodenas, M.; Wirtz, K. Intercomparison of the DOAS and LOPAP techniques for the detection of nitrous acid (HONO). *Atmos. Environ.* **2006**, *40* (20), 3640–3652.

(28) Tsikas, D. Analysis of nitrite and nitrate in biological fluids by assays based on the Griess reaction: Appraisal of the Griess reaction in

the l-arginine/nitric oxide area of research. *J. Chromatogr. B: Anal. Technol. Biomed. Life Sci.* **2007**, *851* (1−2), 51−70.
(29) Huang, G.; Zhou, X.; Deng, G.; Qiao, H.; Civerolo, K. Measurements of atmospheric nitrous acid and nitric acid. *Atmos. Environ.* **2002**, *36* (13), 2225−2235.
(30) Peterson, B. J.; Fry, B. Stable isotopes in ecosystem studies. *Annu. Rev. Ecol. Syst.* **1987**, 18293−320.
(31) Murphy, D. V.; Recous, S.; Stockdale, E. A.; Fillery, I. R. P.; Jensen, L. S.; Hatch, D. J.; Goulding, K. W. T. Gross nitrogen fluxes in soil: theory, measurement and application of ^{15}N pool dilution techniques. In *Adv. Agron.*; Sparks, D., Ed.; Academic Press: Salt Lake City, 2003; Vol. *79*, pp 69−118.
(32) Houlton, B. Z.; Sigman, D. M.; Hedin, L. O. Isotopic evidence for large gaseous nitrogen losses from tropical rainforests. *Proc. Natl. Acad. Sci. U. S. A.* **2006**, *103* (23), 8745−8750.
(33) Green, L. C.; Wagner, D. A.; Glogowski, J.; Skipper, P. L.; Wishnok, J. S.; Tannenbaum, S. R. Analysis of nitrate, nitrite, and [^{15}N]nitrate in biological fluids. *Anal. Biochem.* **1982**, *126* (1), 131−138.
(34) Yakushiji, H.; Kanda, J. Determination of experimentally enriched ^{15}N in nitrate nitrogen based on an improved method of azo dye formation. *J. Oceanogr.* **1998**, *54* (4), 337−342.
(35) Florian Stange, C.; Spott, O.; Apelt, B.; Russow, R. W. B. Automated and rapid online determination of ^{15}N abundance and concentration of ammonium, nitrite, or nitrate in aqueous samples by the SPINMAS technique. *Isot. Environ. Health Stud.* **2007**, *43* (3), 227−236.
(36) Pérez, T.; Trumbore, S. E.; Tyler, S. C.; Matson, P. A.; Ortiz-Monasterio, I.; Rahn, T.; Griffith, D. W. T. Identifying the agricultural imprint on the global N_2O budget using stable isotopes. *J. Geophys. Res.: Atmos.* **2001**, *106* (D9), 9869−9878.
(37) Ozkan, U. S.; Cai, Y. P.; Kumthekar, M. W. Investigation of the reaction pathways in selective catalytic reduction of NO with NH_3 over V_2O_5 catalysts: isotopic labeling studies using $^{18}O_2$, $^{15}NH_3$, ^{15}NO, and $^{15}N^{18}O$. *J. Catal.* **1994**, *149* (2), 390−403.
(38) Nielsen, L. P. Denitrification in sediment determined from nitrogen isotope pairing. *FEMS Microbiol. Lett.* **1992**, *86* (4), 357−362.
(39) Moore, H. The isotopic composition of ammonia, nitrogen dioxide and nitrate in the atmosphere. *Atmos. Environ. (1967−1989)* **1977**, *11* (12), 1239−1243.
(40) Coplen, T. B. Guidelines and recommended terms for expression of stable-isotope-ratio and gas-ratio measurement results. *Rapid Commun. Mass Spectrom.* **2011**, *25* (17), 2538−2560.
(41) Biemann, K. *Mass spectrometry: organic chemical applications*; McGraw-Hill: New York, 1962; pp 223−225.
(42) Caimi, R. J.; Brenna, J. T. Quantitative evaluation of carbon isotopic fractionation during reversed-phase high-performance liquid chromatography. *J. Chromatogr. A* **1997**, *757* (1−2), 307−310.
(43) Lalor, S. T. *Soils of UCD research farm*; University College Dublin: Lyons Estate, Celbridge, Co. Kildare, 2004.
(44) Persson, X.-M. T.; Błachnio-Zabielska, A. U.; Jensen, M. D. Rapid measurement of plasma free fatty acid concentration and isotopic enrichment using LC/MS. *J. Lipid Res.* **2010**, *51* (9), 2761−2765.
(45) Shinn, M. B. Colorimetric method for determination of nitrite. *Ind. Eng. Chem., Anal. Ed.* **1941**, *13* (1), 33−35.
(46) Pai, S.-C.; Yang, C.-C.; P. Riley, J. Formation kinetics of the pink azo dye in the determination of nitrite in natural waters. *Anal. Chim. Acta* **1990**, *232* (0), 345−349.
(47) Lu, L.; Han, W.; Zhang, J.; Wu, Y.; Wang, B.; Lin, X.; Zhu, J.; Cai, Z.; Jia, Z. Nitrification of archaeal ammonia oxidizers in acid soils is supported by hydrolysis of urea. *ISME J.* **2012**, *6* (10), 1978−1984.
(48) Di, H. J.; Cameron, K. C.; Shen, J. P.; Winefield, C. S.; O'Callaghan, M.; Bowatte, S.; He, J. Z. Nitrification driven by bacteria and not archaea in nitrogen-rich grassland soils. *Nat. Geosci.* **2009**, *2* (9), 621−624.
(49) Mobley, H. L.; Hausinger, R. P. Microbial ureases: significance, regulation, and molecular characterization. *Microbiol. Rev.* **1989**, *53* (1), 85−108.
(50) Thornton, F. C.; Shurpali, N. J.; Bock, B. R.; Reddy, K. C. N_2O and NO emissions from poultry litter and urea applications to Bermuda grass. *Atmos. Environ.* **1998**, *32* (9), 1623−1630.
(51) Li, D.; Wang, X. Nitrogen isotopic signature of soil-released nitric oxide (NO) after fertilizer application. *Atmos. Environ.* **2008**, *42* (19), 4747−4754.
(52) Anthonisen, A. C.; Loehr, R. C.; Prakasam, T. B. S.; Srinath, E. G. Inhibition of nitrification by ammonia and nitrous acid. *J. − Water Pollut. Control Fed.* **1976**, *48* (5), 835−852.
(53) Müller, C.; Stevens, R. J.; Laughlin, R. J. A ^{15}N tracing model to analyse N transformations in old grassland soil. *Soil Biol. Biochem.* **2004**, *36* (4), 619−632.
(54) Dong, W.; Hu, C.; Zhang, Y.; Wu, D. Gross mineralization, nitrification and N_2O emission under different tillage in the North China Plain. *Nutr. Cycl. Agroecosyst.* **2012**, *94* (2−3), 237−247.
(55) Santoro, A. E.; Sakamoto, C. M.; Smith, J. M.; Plant, J. N.; Gehman, A. L.; Worden, A. Z.; Johnson, K. S.; Francis, C. A.; Casciotti, K. L. Measurements of nitrite production in and around the primary nitrite maximum in the central California Current. *Biogeosciences* **2013**, *10* (11), 7395−7410.
(56) Buchwald, C.; Casciotti, K. L. Isotopic ratios of nitrite as tracers of the sources and age of oceanic nitrite. *Nat. Geosci.* **2013**, *6* (4), 308−313.